ORIGINAL ARTICLE

Thermal streak spacing in fully developed duct flow with different Reynolds and Prandtl numbers

Mohit Pramod Sharma[1] · **Iztok Tiselj[1,2]** · **Jan Kren[1,2]** · **Blaž Mikuž[1]** · **Leon Cizelj[1,2]**

Abstract

The present study investigates the behaviour of thermal streaks on a heated foil which is cooled with turbulent flow in a square duct channel. Real-time infrared thermography is used to visualize and measure the spacing between the thermal streaks. A stainless-steel foil with a thickness of 25 microns is cooled by water. The experiments were performed in a range of Reynolds numbers from 5000 to 20000 and Prandtl numbers from 3 to 7. The mean temperature, root-mean-square of temperature and autocorrelation function have been calculated and used to measure the average thermal streak spacing and power spectra in the spanwise and streamwise directions. The root mean square temperature was 0.3 °C to 0.5 °C which corresponds to roughly 10% of the mean temperature difference between foil and water. The uncertainty in mean temperature difference and root mean square temperature was around 5% and 10%, respectively. The measured thermal streak spacing was 100 wall unit to 180 wall unit under the present experimental range. The uncertainty in measured thermal streak spacing was around 2.5%. The effects of Reynolds number, Prandtl number and heat flux on the thermal streak spacing and also on the statistics of the temperature field have been presented and discussed in this paper. A new correlation has been proposed to predict the dimensionless thermal streak spacing. The error in the prediction is estimated within ± 15 %.

Abbreviations

K	Thermal activity ratio, dimensionless	V	Axial velocity, m/s
ρ	Density, kg/m3	C	Counts, dimensionless
C_p	Specific heat, J/kgK	D	Hydraulic diameter, m
k	Thermal conductivity, W/mK	Re	Reynolds number, dimensionless
T	Temperature, °C	Re_τ	Friction Reynolds number, dimensionless
T'	Instantaneous temperature, °C	Pr	Prandtl number, dimensionless
$\overline{T}$	Mean surface temperature, °C	τ_ω	Wall shear stress, N/m²
T_τ	Friction temperature, °C	L	Length of foil, m
u^*	friction velocity (m/s)	ΔP	Pressure drop, N/m²
		P_s	Perimeter (m).
		ϑ	Kinematic viscosity of the fluid, m²/s
		Q	Heat flux, W/m²
		R_x	Autocorrelation function in x direction, dimensionless
		T	Time, s
		Λ	Thermal streak spacing, m
		λ^+	Dimensionless thermal streak spacing, dimensionless
		μ	Dynamic viscosity, N-s/m²
		E	Error, dimensionless
		ME	Mean error, dimensionless
		$RMSE$	Root Mean Square Error, dimensionless

Subscripts

F	Fluid
W	Wall

✉ Mohit Pramod Sharma
mohit.lucky07@gmail.com

Iztok Tiselj
iztok.tiselj@ijs.si

Jan Kren
jan.kren@ijs.si

Blaž Mikuž
blaz.mikuz@ijs.si

Leon Cizelj
leon.cizelj@ijs.si

1   Reactor Engineering Division, Jožef Stefan Institute, Jamova cesta 39, 1000 Ljubljana, Slovenia

2   Faculty of Mathematics and Physics, University of Ljubljana, Jadranska 19, Si-1000 Ljubljana, Slovenia

FW   Foil-water
RMS   Root mean square
Ex   Experiment
Pr   Predicted
x, y, z   The coordinate axis x, y and z correspond to streamwise, wall-normal and spanwise direction

1 Introduction

Conjugate heat transfer phenomena occur in most engineering applications which involve heat transfer between solids and fluids. In conjugate heat transfer, the temperature fluctuations at the fluid-solid wall boundary are of great importance to the design and safety of the system. The temperature fluctuation is due to turbulent vortical structures near the wall giving rise to the spatio-temporal turbulent heat transfer. Generally, thermocouples have been used to measure the time average temperature which ignores the unsteady nature of heat transfer. Hence, the knowledge of unsteadiness is required to better comprehend the physics of heat transfer and to increase the precision of the thermal design of heat transfer equipment. Temperature fluctuations in the fluid can enter into the solid wall depending on the thermal boundary condition giving rise to thermal fatigue and failure of the components [1].

The temperature fluctuations in the fluid mainly depend on the heat capacity and thermal conductivity of both the fluid and the solid. Thus, a thermal activity ratio (K) is defined as the ratio of the product of the thermal conductivity and heat capacity of the fluid to the product of thermal conductivity and heat capacity of the solid [2, 3], which is mathematically represented as

$$K = \sqrt{\rho_f C_{pf} k_f \Big/ \rho_w C_{pw} k_w} \tag{1}$$

The thermal activity ratio determines whether the temperature boundary condition at the wall is fluctuating or non-fluctuating [4]. If the thermal activity ratio K is equal to zero and the wall thickness is greater than zero then the temperature fluctuations in the fluid cannot enter into the wall and is known as a non-fluctuating temperature boundary condition. If the thermal activity ratio K is equal to infinity, temperature fluctuations in the fluid can enter into the wall and is known as a fluctuating temperature boundary condition. The fluctuating temperature boundary condition does not depend upon the thickness of the wall. These two boundary conditions are ideal and the actual boundary conditions lie in between the two ideal cases.

Figure 1 shows a hot wall cooled by adjacent turbulent flow. The red regions over the foil represent high temperature, while the yellow regions represent temperature lower than the mean temperature value ($\bar{T}$). The patterns of high and low-temperature regions are called thermal streaks. These streaks are present in the near-wall turbulent flow [5] and can be visualized when heat is added to the foil. The lower velocity regions will emerge as high-temperature streaks and the higher velocity regions will be seen as low-temperature streaks as the local heat transfer coefficients are different over the streaks, which creates low and high-temperature zones over the foil.

To study the nature of turbulence near the wall in a turbulent flow, an experiment was first carried out by Boussinesq [6] in 1868. In his experiment, air (Pr < 1) was used as the working fluid. He noted that the streaks appear near the surface of the solid and showed the regions of high and low velocities in the fluid.

Fig. 1 Mechanism of thermal streaks formation on the foil
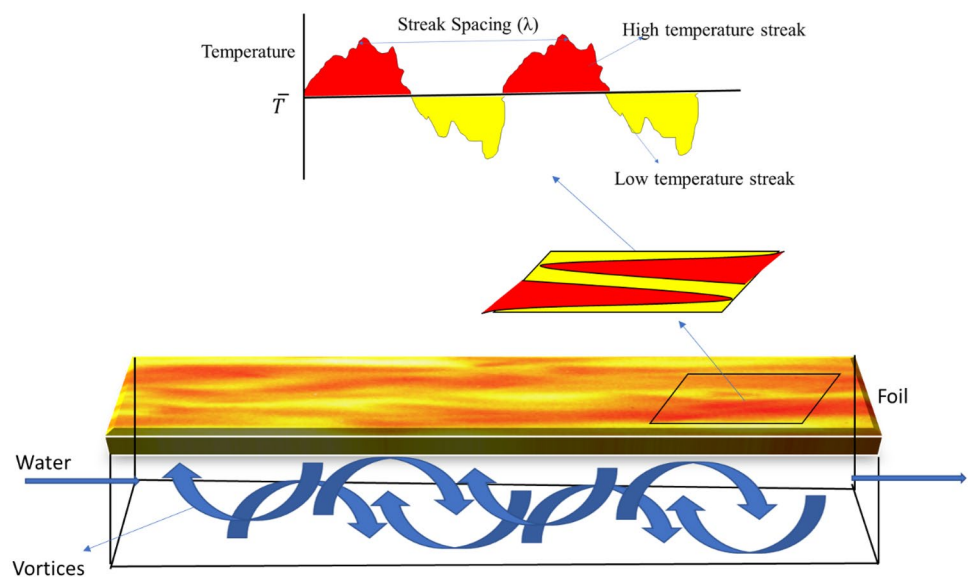
Iritani et al. in 1985 [7] conducted the experiment with water at a fixed Reynolds number of around 6300 and a Prandtl number of 6.8. The liquid crystal technique and hydrogen bubble method were used in their experiments. The liquid crystal technique was used to visualize the wall temperature fluctuations on a thin stainless-steel foil (30 μm) while the hydrogen bubble method was used to visualize the flow structure. It was observed that the high-temperature streaks are correlated with the low-velocity streaks and vice versa.

Hetsroni et al. in 1994 [8] conducted experiments with water flowing in a flume. The Reynolds numbers were between 5000 and 10000, while the Prandtl number was fixed at 6.8. The infrared thermography was used to observe the temperature streaks on the constantan foil surface having a thickness of 50 μm. It was found that the dimensionless thermal streak spacing depends on the Reynolds number. The dimensionless thermal streak spacing increases with increasing Reynolds number. The maximum amplitude of wall temperature fluctuations was found to be ± 40% of the difference between the average wall temperature and the fluid bulk temperature. Hetsroni et al. in 1996 [9] conducted experiments to study the heat transfer coefficient and temperature distribution near a single polystyrene particle at the thin constantan wall surface (50 μm). Water was used as a working fluid. The Reynolds numbers were between 5000 to 10000 while the Prandtl number was equal to 7. A sharp increase in the heat transfer coefficient was observed in front of the single polystyrene particle, where the heat-transfer coefficient was found to be more than three times in the zone without polystyrene particle Moreover, the amplitude of temperature fluctuations in front of the particles exceeds that of the undisturbed flow.

Hetsroni et al. in 1997 [10] conducted an experiment with water flowing in a flume. The Reynolds numbers were between 7000 to 20000 while the Prandtl number was equal to 7. The authors [10] studied the effect of a drag-reducing surfactant on the nature of turbulence near the wall. The surfactant used in the experiment to reduce the flow resistance was the Habon G solution. Infrared thermography was used to visualize and measure the spanwise spacing between the thermal streaks over the thin constantan foil surface (50 μm). A correlation was proposed to calculate the average streak spacing which is a linear function of the friction Reynold number.

Mosyak et al. in 2001 [11] conducted experiments to study the temperature fluctuations for two thermal boundary conditions. The first case of wall boundary conditions is constant axial heat flux and quasi peripheral isothermal condition (H1), and the second case is constant axial heat flux and quasi peripheral isoflux condition (H2). The Reynolds number varied from 10000 to 20000, while the Prandtl number was fixed to 4. For the first case (H1), experiments

were conducted with water flowing over a 20 mm thick copper plate (flume) whereas, for the second case (H2), experiments were conducted with water flowing over a 50 μm thin stainless-steel foil (rectangular channel). It was found that the mean thermal streak spacing in both cases is independent of thermal entrance length. However, the root-mean-square (RMS) temperature found to be larger in the case of the H2 as compared to the H1 conditions.

Nakamura and Yamada in 2013 [12] studied the spatiotemporal variation of heat transfer by using infrared thermography. The air was used as fluid (Prandtl number <1) flowing over a heated thin titanium foil (2 μm). It was found that the temperature fluctuations on the foil are diminished in time and space. This is due to thermal inertia and lateral heat conduction. However, it can be recovered by solving the inverse heat conduction equation. Shiibara et al. in 2017 [13] conducted experiments with water to study the fluctuations of heat transfer coefficient on a heated thin titanium foil (40.6 μm) in a pipe flow during sudden opening and closing of a valve using infrared thermography. The Reynolds numbers were set to 12,000 and 3000 while the Prandtl number was kept constant at 5.4. The valve opening time was half of the total time. It was found that the heat transfer coefficient is increased just after the deceleration of the flow rate and reduced just after the acceleration of the flow rate. Similar experiments were conducted by Nakamura et al. in 2020 [14] to investigate delay response in the heat transfer enhancements due to a change in Reynolds number. The Reynolds numbers varied from 7000 to 21000 and then from 21000 to 7000 while the Prandtl number was kept constant at about 5.4. Tiselj et al. in 2021 [15] performed experiments and numerical simulations to investigate the temperature fluctuation in a turbulent flow at fixed Reynold numbers of 10000 and Prandtl of 5.4. A stainless-steel foil with a thickness of 25 μm and water used as a working fluid. The measured half thermal streak spacing in the spanwise direction was found to be 60 wall units.

It can be concluded that the experiments were performed for various Reynolds numbers, while the Prandtl number effect was not examined. There is a lack of experimental studies, which cover a wide range of Reynolds and Prandtl numbers; more precisely, there are no experiments covering a range of Prandtl numbers at a fixed Reynolds number. Therefore, it is important to investigate the effects of the Reynolds and Prandtl number on the thermal streak spacing. In addition, the effect of the heat flux magnitude on the thermal streak spacing should be investigated as well.

In this work, experiments were carried out to investigate the thermal fluctuations on a heated metal foil in the case of turbulent duct flow. The present study aims to measure the thermal streak spacing on a heated foil cooled with a turbulent flow in a square duct. Infrared thermography is used to visualize and measure the distances between thermal streaks.
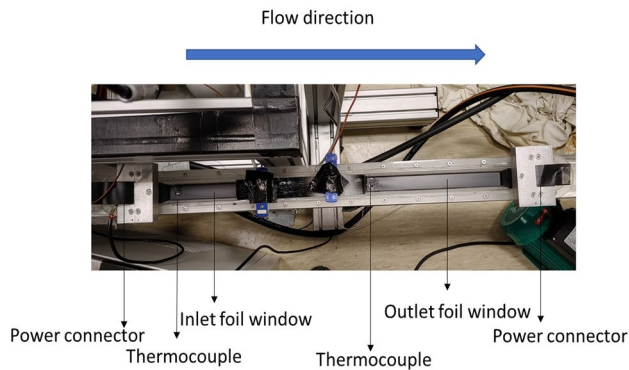
Fig. 2 Top view of the measuring window (IR camera facing) of the test section

A stainless-steel (SS) foil with a thickness of 25 microns and water is used as the working medium. The experiments were performed in a range of Reynolds numbers from 5000 to 20000 and Prandtl numbers from 3 to 7. The thermal activity ratio is 0.21 for the entire range of Reynolds and Prandtl numbers. The effects of Reynolds number, Prandtl number, and heat flux on the statistics of the temperature field, thermal streak spacing and power density have been presented and discussed in this article. A new correlation is also proposed for predicting the dimensionless thermal streak spacing, which is shown to be a function of Reynolds number and Prandtl number.

2 Experimental facility

2.1 Test section

The experimental test rig used in this study is situated at the THELMA laboratory (Reactor Engineering Division, Jožef Stefan Institute, Ljubljana, Slovenia). The experimental test rig has been designed and installed to study the thermal fluctuations in a single-phase turbulent flow. Figure 2 shows the measuring window section (inlet and outlet measuring window with thermocouples and power connectors

assembly) of the whole test section. The test section is made of smooth acrylic glass having a wall thickness equal to 15 mm. The square duct has a cross-section with a dimension of 30 mm×30 mm. The length of the test section is 4000 mm, which is sufficient to attain a fully developed flow and temperature field. According to the literature [11, 16], the fully developed length for turbulent flow should be 100 times the hydraulic diameter and the thermal entrance length for turbulent flow should be 10 times of the hydraulic diameter [17]. The temperature measurements are obtained at the inlet window (100 mm × 20 mm) and also at the outlet window (200 mm × 20 mm) which are located at 2700 mm and 3000 mm from the inlet of the test section.

2.2 Test rig

The experimental test rig, shown in Fig. 3, consists of a test section (explained in Section 2.1), a thermal bath, a centrifugal pump, an electrical load controller (ELC), a water filter, a DC power supply and valves. The instruments used in the present loop were a Coriolis flow meter, thermocouples, thermometer and differential pressure transmitter (DPT).

The thermal bath (LAUDA-845C) keeps a stable temperature in the water loop. The accuracy of the thermal bath is 0.1 °C. The pump can deliver a water flow at the rate of 45 m³/h or a head of 34 m. Control valves are used to adjust the flow rate from 0.08 to 0.35 kg/s. The corresponding Reynolds number is around 5000 to 20000. The DC power supply of 12 V and 120 Ah battery is used for resistance heating of the SS foil. The ELC (EA-EL 3160-60 A) is used for power control, the voltage and electric current range are 160 V (accuracy < 0.1%) and 60 A (accuracy < 0.2%), respectively. The flow rate is measured with the Coriolis flow meter (micro motion elite CMFS). The accuracy of the Coriolis flow meter is ±0.5% of the measured value. Water temperature at the inlet and at the outlet of the test section is measured by a T-type thermocouple having a range of up to 200 °C with an accuracy of ±1 °C and a mercury thermometer (accuracy of ±0.1 °C). In order to measure the surface temperature of the foil, fine thermopile was welded on the foil at the outlet and inlet measuring window. The thermopile and T-type thermocouple are connected to the
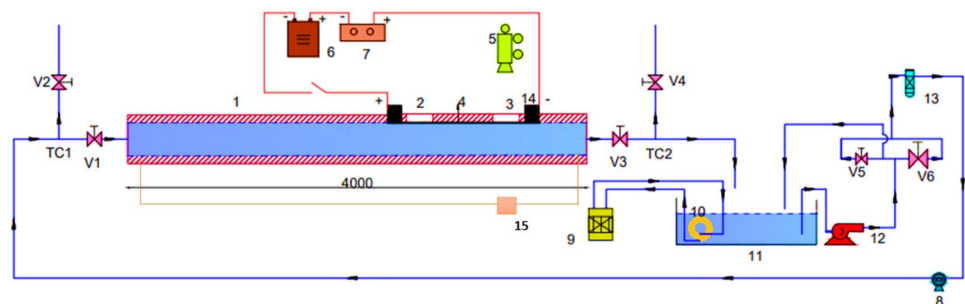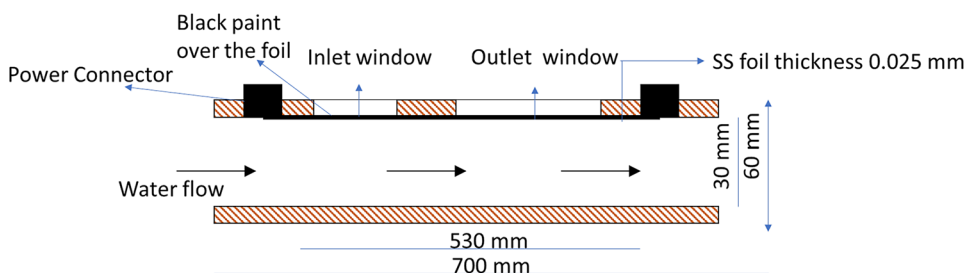
Fig. 3 Experimental test rig

Fig. 4 Heated foil section

K170 water triple point reference to provide an accurate temperature measurement on the absolute scale. The accuracy of the K170 water triple point reference is ±0.02 °C. The pressure drop is measured by a differential pressure transmitter. The distance between the inlet pressure measuring and the outlet-pressure measuring point is 3700 mm before the outlet of the test section. The upper range of differential pressure transmitter 266MST-ABB can be varied from 2 to 60 mbar. In the experiment, the DPT was set to the range from 0 to 5 mbar with an accuracy of ± 0.11%,

Figure 4 shows the heated portion of the test section. Resistance heating was applied to the SS foil, stuck with a thin silicon layer to the lower part of an acrylic frame. The thickness of the SS foil (DIN EN 1.4301 SS) is 25±2 μm. The SS foil has density of 7900 kg/m^3, thermal conductivity of 15 W/m-K and specific heat capacity of 500 J/kgK. The actual electrical resistance of SS foil was measured which is around 0.60 Ohm. A multimeter is used for measuring voltage (20-220 V) across the foil. The accuracy of the multimeter is ± 0.5 %. The outer surface of the foil is painted with black paint having a thickness of 20±10 μm, which reduces the reflectivity of the SS foil and enables temperature measurement by the infrared (IR) camera.

The fast-infrared camera (FLIR-X6901sc SLS) is used to study the temperature field. The system software converts the counts to temperature assuming the emissivity of the target object, the reflected (or background) temperature and the ambient temperature. However, an accurate emissivity value is difficult to obtain and also depends on the viewing angle, the reflected temperature and the ambient temperature. In addition, the sensitivity of an IR camera is 40 mK, however, the accuracy of the absolute temperature is ±1 °C from 0 °C to 3000 °C which is up to 5 % in our experimental measurement range from 20 °C to 50 °C. However, this measurement error can be reduced by a calibration procedure. Therefore, instead of adjusting emissivity, the IR counts were calibrated with the temperature measured by a thermocouple calibrated with 0.1 °C accuracy in the relevant temperature range. To protect the IR camera from ambient radiation, a paper shield is provided around the camera and the foil. Calibration runs were performed under isothermal conditions and sufficient duration (more than 5 min) for the range from 20 °C to 55 °C as shown in Fig. 5.

A linear fit is obtained between counts (*C*) and temperature (*T* in °C) which is as follows

$$C = 48.80\,T + 2334.5 \qquad (2)$$

Absolute error in predicted temperature in Eq. (2) is around ± 1.6 % and Root Mean Square Error (RMSE) is 0.21 % except for some points below 25 °C which show an error of + 2.1 % and RMSE of 1.4 %. Hence, by using the calibration method, gives more accurate results.

3 Experimental matrix and test procedure

The experimental matrix is shown in Table 1.

The experiments were performed to investigate the effect of Reynolds number, Prandtl number and heat flux. The experiments were performed for Re of 5000 to 20000 and Pr of 3 to 7. The lower Reynolds number of 5000 roughly corresponds to the bottom limit of a fully developed turbulent flow in a channel while the upper range Re of 20000 shows the maximum capability of our system i.e. thin foil was used in the experiment which cannot withstand high
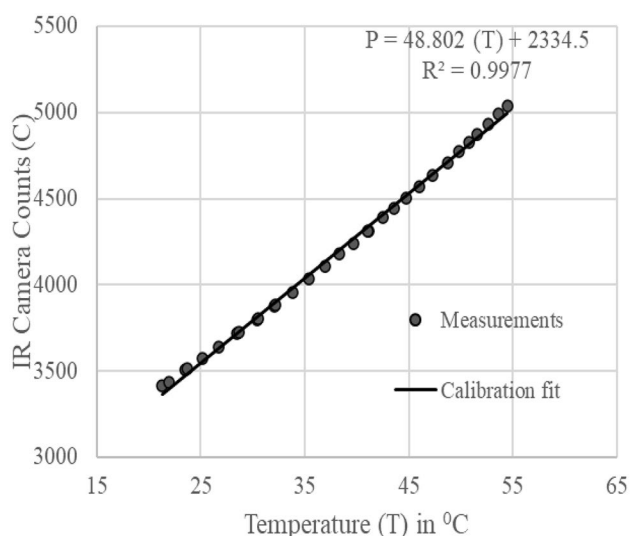

Fig. 5 Calibration fit for IR camera count against thermocouple temperature

Table 1 Experimental matrix

Reynolds number (Re)	Prandtl number (Pr)						
5000	3.5	3.9	4.4	4.8	5.4	6	6.6
10000	3.5	4	4.4	4.8	5.4	5.9	6.6
15000	3.5	4	4.4	4.75	5.4	/	/
20000	3.5	3.9	/	/	/	/	/

flow pressure. Also, above Re of 20000, it is difficult to obtain minima in the autocorrelation function (due to an insufficient pixel resolution of IR camera), since the spacing of streaks becomes much finer with the increase in the Reynolds number. Each run had been performed for two different heat fluxes such that the temperature difference between foil and water are around 5 °C and 3 °C, respectively. The overall temperature difference between foil and water was maintained low (up to 5 °C) in order to satisfy the condition of temperature being a passive scalar [15]. A passive scalar quantity is independent of the viscosity and density of the fluid.

Water in the tank was maintained at a constant temperature using the thermal bath and the heat exchanger. The water flows into the test section by pump via the water filter and valve V1. It is discharged from the test section through valve V3 (refer to Fig. 3). The flow rate is gradually increased by controlling valves V5 and V6. The V5 is smaller than V6 and was provided for fine-tuning of flow rate. The valves V2 and V4 are used for venting out the trapped air bubbles in the system. The temperature at the inlet and the outlet were measured by thermocouples TC1 and TC2 respectively. The water flow rate was measured by a Coriolis flow meter before entering the test section. After achieving the desired flow condition, the DC electric heating was switched on. The electric current heats the foil and thermal streaks on the surface of the foil were captured using a high-speed IR camera as shown in Fig. 6.

In the experiment, a high-speed IR camera was mounted perpendicular to the foil with a small tilt of 10 degrees to avoid self-reflection from the foil to the camera sensor. Also, to avoid the edge effect and thermocouple effect; slightly smaller measured windows with a size of 185 mm × 18 mm instead of 200 mm × 20 mm for outlet window and 80 mm × 18 mm instead

of 100 mm × 20 mm for inlet window represented by white border-box (Fig. 6) were analyzed. The resolution of the IR camera is 640×512 pixels, while the pixel over the foil was approximately 60 pixel x 620 pixel for the outlet window and 100 pixel x 500 pixel for the inlet window along the width and length of the foil, respectively. The IR camera was operated at a frequency of 15 Hz for 5 minutes which produce 4500 instantaneous IR images. IR camera is also a cause of experimental uncertainty. RMS temperature fluctuations of the unheated foil are found to be around 0.05 °C to 0.07 °C for the range of 20 °C to 50 °C respectively.

In addition to the above, pressure drop was measured by DPT for every run and has been assessed by pressure drop correlations as shown in Fig. 7.

For evaluation, the experimental pressure drop is compared with the predicted pressure drop by existing models such as the Moody [18] chart, Blasius [19] correlation and Filonenko [20] correlation. Error analysis has been performed to estimate the maximum error, minimum error and mean error (ME) and is calculated by using the equation as follows.
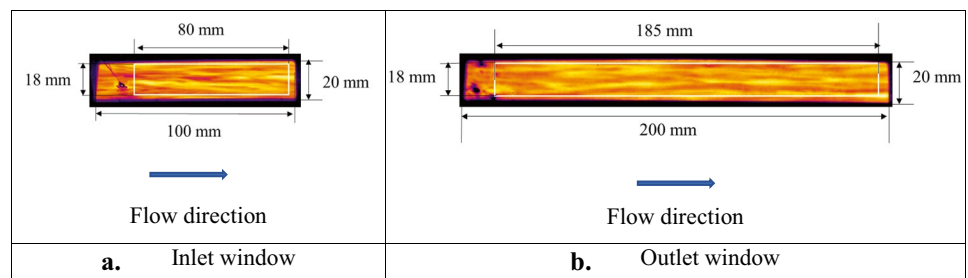
$$E_{max} = max\left(\frac{\Delta P_{pr} - \Delta P_{ex}}{\Delta P_{ex}} \times 100\right)\% \qquad (3)$$

$$E_{min} = min\left(\frac{\Delta P_{pr} - \Delta P_{ex}}{\Delta P_{ex}} \times 100\right)\% \qquad (4)$$

$$ME = \left(\frac{\sum_{i=1}^{n} E_i}{n} \times 100\right)\% \qquad (5)$$

Where n is number of pressure drop data points and $E_i = \frac{\Delta P_{pr}^i - \Delta P_{ex}^i}{\Delta P_{ex}^i}$

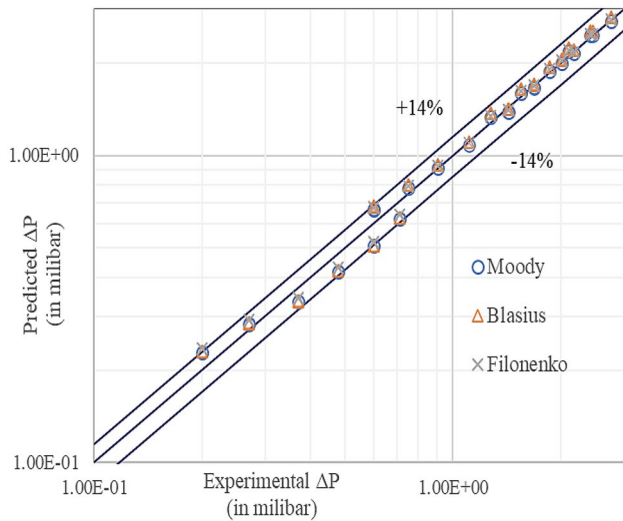**Fig. 6** Infrared images at measuring window during heating

a. Inlet window   b. Outlet window

Fig. 7 Validation of experimental pressure drop against pressure drop correlations

Table 2 Error analysis of experimental data against pressure drop (ΔP) correlation

Correlation for ΔP	Max error %	Min error %	Average error %
Moody [18]	+11.4	-9.9	+1.2
Blasius [19]	+14	-9.4	+3.2
Filonenko [20]	+13.7	-7.3	+3.0

$$Re_\tau = \rho^* D/\mu \tag{6}$$

$$Re = \rho V D/\mu \tag{7}$$

Where ρ is the density of fluid (kg/m^3), D is the hydraulic diameter (m), V is the axial velocity (m/s) and $u^*(= \sqrt{\tau_\omega/\rho})$ is the friction velocity (m/s). τ_ω is the wall shear stress (N/m^2) which is calculated from the measured pressure drop.

Figure 8 shows the comparison of friction Reynolds number in the present experiments with the experiments of Vinuesa et al. [21] and Uhlmann et al. [22] which were specifically performed for square duct. Vinuesa et al. [21] experiments were limited to Re of 5700 while Uhlmann et al. [22] were limited to Re of 2500. However, Uhlmann et al. [22] found it to be in good agreement with empirical correlation [23]. Our experimental range varied from Re of 5000 to 20000. Hence, Vinuesa et al. [21] and Uhlmann et al. [22] data interpolated into our experimental range. It is expected that an increase in Re increases Re$_\tau$ as the friction

The error analysis shows how much measurement values differ from the predicted values of the models considered. Table 2 shows all correlation prediction errors with respect to the measured pressure drop from experiments.

All experimental data is well in the prediction range of all correlations (within ± 14 %) and the average error is below 3.2 %.

Figure 8 shows the plot of friction Reynolds number (Re$_\tau$) against the bulk Reynolds number (Re). The friction Reynolds number and Reynold number are calculated as follows.

Fig. 8 Plot of friction Reynolds number against bulk Reynolds number and its comparison with the experiments of Vinuesa et al. [21] and Uhlmann et al. [22]
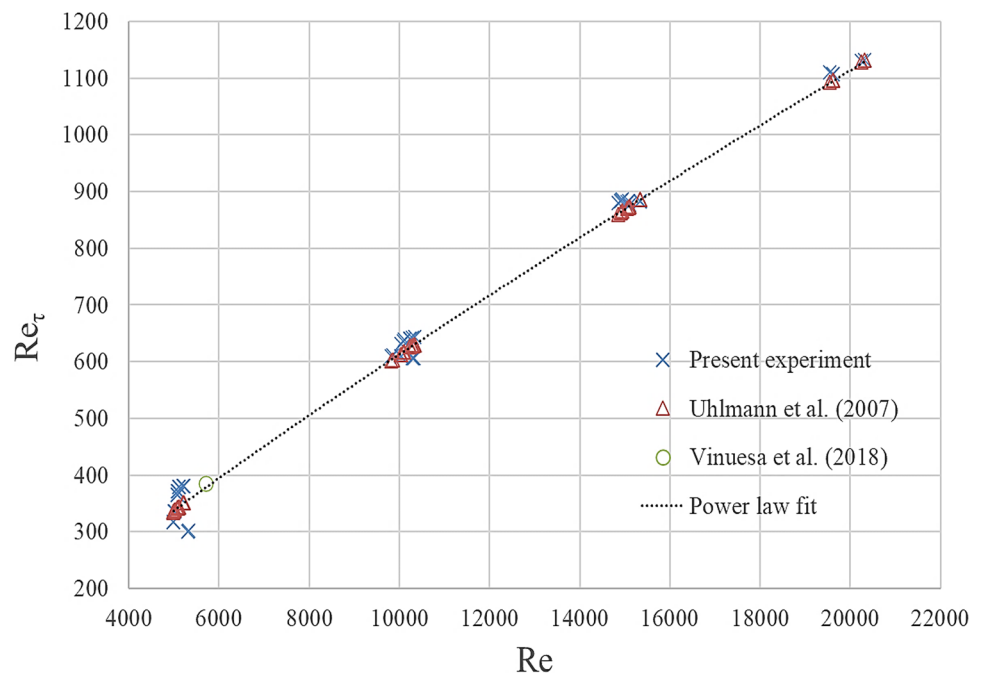
velocity increases with an increase in the pressure drop. The error between the present experiments and the experiments of Vinuesa et al. [21] and Uhlmann et al. [22] are within ± 7% except at Re of 5000 where it shows ± 18%. It can observe much better agreement of our measurements at Re greater than equal to 10000 than at Re of 5000. It attributes larger uncertainties at Re of 5000 to the transitional nature of such flow. It is well known [23] that analyses of flows at Re between 2000 and 5000 are particularly difficult due to the chaotic nature of the laminar to turbulent flow transition. However, the Jones correlation [24] is used for calculating friction velocity in the present paper which has less error (± 5%) as compared to the error (± 18%) in the measured experimental data.

4 Results and discussion

A python code is developed to calculate mean temperature, RMS temperature fluctuations, thermal streak spacing and power spectra from the IR images taken during the experimental run.

4.1 Mean temperature difference (ΔT_{FW}) between the foil and water and RMS temperature fluctuations

The mean temperature ΔT_{FW} is the difference between the mean surface temperature of the foil and water. It can be represented as follows.

$$\Delta T_{FW} = \overline{T} - T_W \tag{8}$$

The error in the ΔT_{FW} is within ± 5 %.

Figure 9 shows the normalized ΔT_{FW} (normalized to friction temperature T_τ) as a function of Prandtl number in the range from 3.6 to 6.8 for different Reynolds numbers between 5000 and 20000. Friction temperature (T_τ) can be calculated as follows.

$$T_\tau = \frac{Q}{\rho C_p u *} \tag{9}$$

Normalized ΔT_{FW} is found to be slowly growing with increase in the Prandtl number for Reynolds number from 5000 to 20000. The reason behind it is that when the Prandtl number is small, it means that the heat diffuses quickly compared to the velocity (momentum) which means lower ΔT_{FW} for lower Prandtl number and vice versa. Also, ΔT_{FW} has the highest value at Re of 5000. Large ΔT_{FW} can be attributed to the reduced heat transfer coefficient. Thus, our results suggest that heat transfer deteriorates at a low Reynolds number of 5000, which could be due to the laminarization of the turbulent flow.

The root-mean-square temperature fluctuations T_{RMS} are calculated by using measured instantaneous temperature and mean surface temperature. The equation for RMS temperature can be represented as follows

$$T_{RMS} = \sqrt{\frac{\sum_1^n \left(T' - \overline{T}\right)^2}{n}} \tag{10}$$

The error in the T_{RMS} is within ± 10 %.

Figure 10 shows the normalized T_{RMS} (normalized with T_τ) as a function of the Prandtl number in the range from 3.6 to 6.8 for different Reynolds numbers between 5000 and 20000

It can be observed that the RMS temperature is found to be increasing with the increase in the Prandtl number. A similar
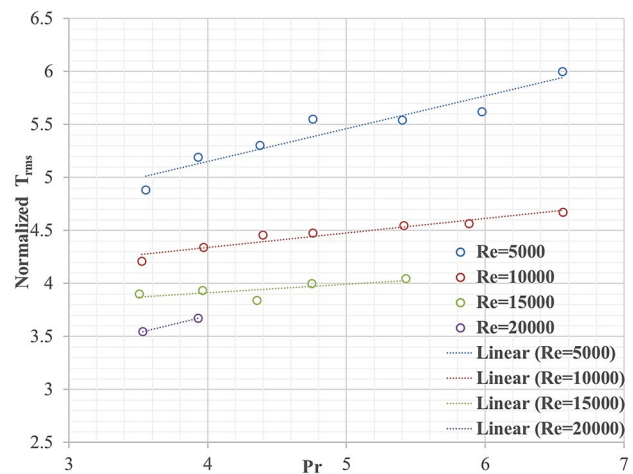

Fig. 9 Normalized mean ΔT_{FW} for different Reynolds number against the range of Prandtl number

Fig. 10 Normalized T_{RMS} against the Prandtl number for different Reynolds numbers
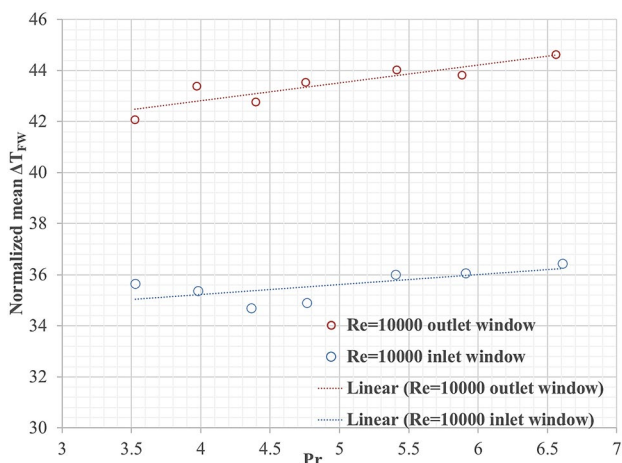
Fig. 11 Comparison of normalized mean temperature between foil and water temperature for outlet vs inlet window

trend is found in the literature [25], which reports increasing temperature fluctuations with the increase in the Prandtl number for fixed Reynolds number. Moreover, the normalized T_{RMS} increases with decreasing Reynolds number.

Figure 11 and Fig. 12 show a comparison of the outlet window and the inlet window. The outlet window shows the larger ΔT_{FW} and T_{RMS} as compared to the inlet window. It could be due to the flow which is not fully thermally developed at the inlet window.

4.2 Effect of Reynolds number, Prandtl number and heat flux on thermal streak spacing and power spectra

Thermal streak spacing As shown in Fig. 6, the patterns of high and low-temperature regions are called thermal streaks which are present in the near-wall turbulent flow.
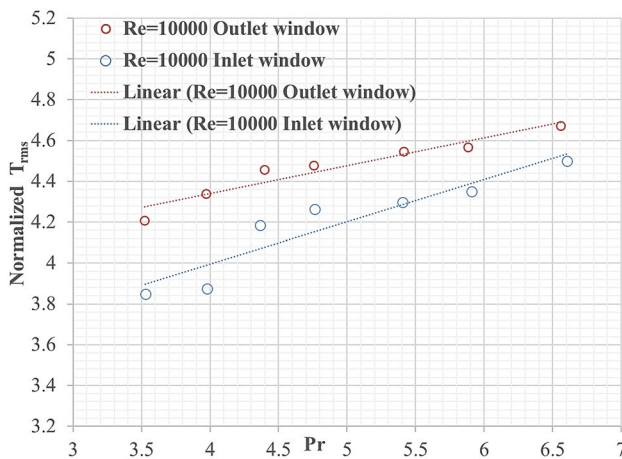
Fig. 12 Comparison of normalized RMS temperature for outlet vs inlet window
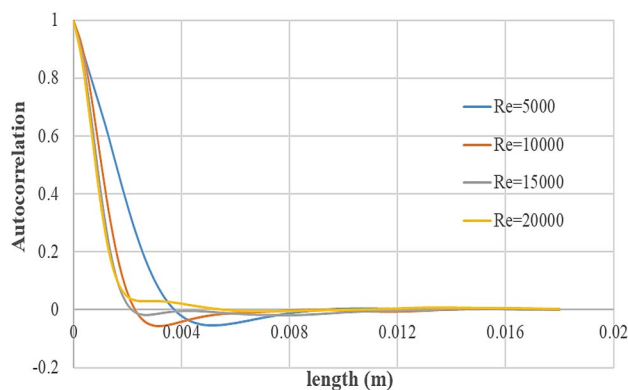
Fig. 13 Effect of Reynolds number on spanwise autocorrelation function

The high-temperature streaks are due to low velocity regions while the low-temperature streaks are due to high velocity regions. The streak spacing is analyzed by using autocorrelation functions and has been often used by previous authors [10, 15]. The autocorrelation is generally used to compare the waveform of the oscillation quantity like velocity, temperature etc. Thus, the same methodology is used for the determination of the thermal streak spacing (λ). The autocorrelation function (R_x) is defined as follows.

$$R_x = \frac{1}{tL_z} \int_0^t \left(\int_0^{L_z} \left(\frac{1}{L_x \sigma^2} \int_0^{L_x} \left(T'_{c,y,z,t} - \overline{T_{x,y,z}} \right) \right. \right.$$
$$\left. \left. \left(T'_{c+x,y,z,t} - \overline{T_{c+x,y,z}} \right) dc \right) dz \right) dt \tag{11}$$

The thermal streak spacing is defined as the distance between the origin and the first minimum in the autocorrelation function (R_x).

Power Spectra The power density is calculated by Fourier transform of the autocorrelation function as follows.

$$powerdensity(x) = \frac{2L_x}{N_L} \left(FFT \left(R_x \right) \right) \tag{12}$$

Figure 13 shows the effect of the Reynolds number on thermal streak spacing in a spanwise direction at a fixed Prandtl number of 3.9. The spanwise autocorrelation function is defined by the distance between the origin and the first minimum in the autocorrelation function (R_x).

Figure 13 shows that an increase in the Reynolds number decreases the thermal streak spacing and vice versa. The decrement in the thermal streak spacing is more pronounced when the Reynolds number changes from 5000 to 10000. This might be due to the flow at Re of 5000 being nearly turbulent. It is also observed in the experiments, that the spacing between streaks is larger and the speed of streaks is rather slow as compared to other Reynolds numbers.
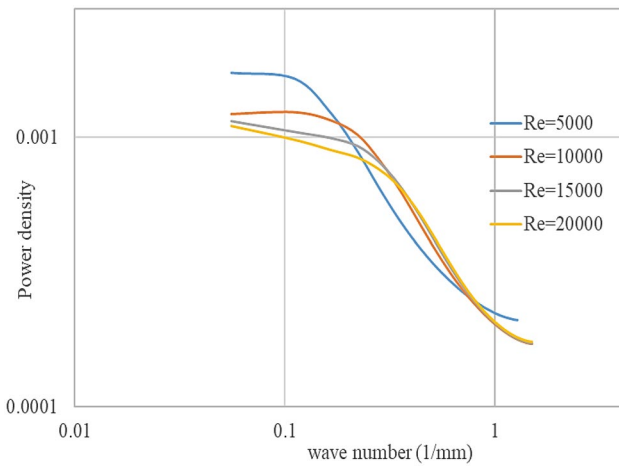
Fig. 14 Effect of Reynolds number on spanwise power density

Figure 14 shows the effect of the Reynolds number on the power spectra in a spanwise direction. The boundary condition is the same as discussed above (Re of 5000 to 20000 and Pr of 3.9). The same trend is expected as discussed in the case of thermal streak spacing with Reynolds number. As power density is nothing but the Fourier transform of autocorrelation function. Hence, it also decreases with an increase in the Reynolds number and vice versa.

Figure 15 (a) shows the effect of the Prandtl number on thermal streak spacing in a spanwise direction. The two extreme Prandtl numbers are taken for comparison. The Prandtl numbers were 3.6 and 6.8 while the Reynolds number was fixed at 10000 in both runs.

It is found that the thermal streak spacing depends on the Prandtl number. The spanwise autocorrelation function slightly decreases with a decrease in the Prandtl number. For a lower Prandtl number, the thermal diffusion rate is close to the momentum diffusion rate, which transfers more energy from mean shear to turbulent fluctuations. Hence there is a slight decrement in thermal streak spacing with a decrease in the Prandtl number. The same trend is found in the power density that the power density decreases with a decrease in the Prandtl number shown in Fig. 15 (b).
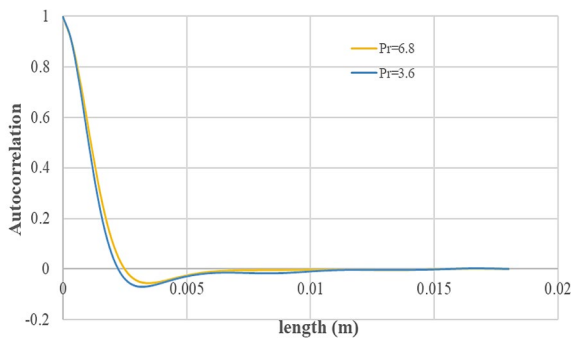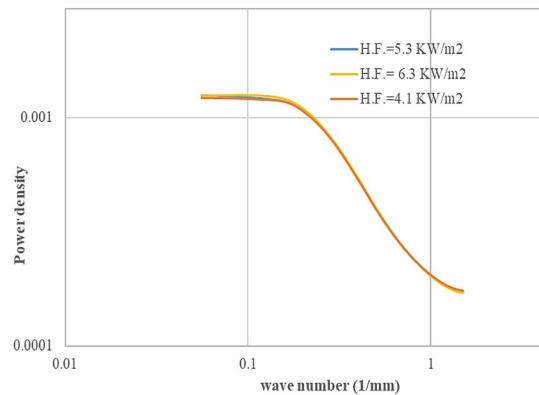

(a) Spanwise autocorrelation function
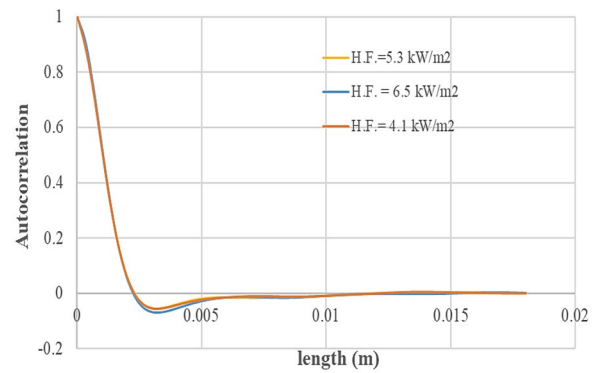
(a) Spanwise autocorrelation function
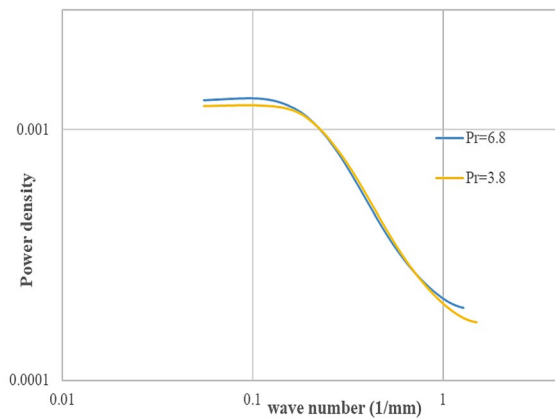
(b) Spanwise power density

(b) Spanwise power density

Fig. 15 Effect of Prandtl number on autocorrelation function and power density

Fig. 16 Effect of heat flux on autocorrelation function and power density
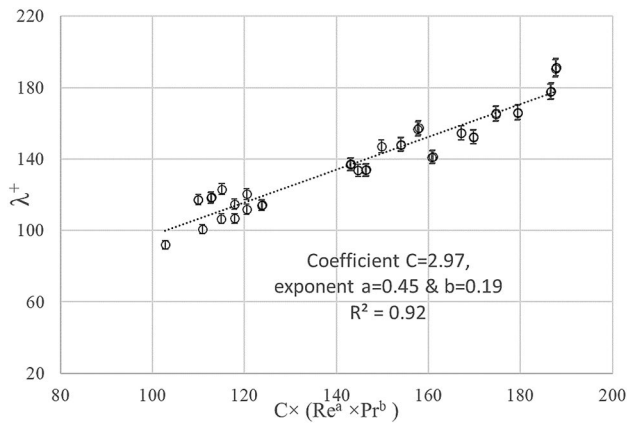
Fig. 17 Plot of dimensionless thermal streak spacing against the Reynolds number and the Prandtl number

Figure 16(a) and (b) shows three heat fluxes of 4.1 kW/m², 6.5 kW/m² and 5.3 kW/m² with fixed Re of 10000 and Pr of 3.6. It can be seen that the heat flux does not have any effect on the thermal streak spacing and power density. This is an expected results for ideal passive scalar fields, which turns out to be very good approximation also in our experiment, where turbulence remains almost unaffected by the temperature field.

4.3 Development of correlation

As discussed in Sect. 4.2, the thermal streak spacing is found to be dependent on the Reynolds number and the Prandtl number, however, it is independent of heat flux. Hence, a correlation for dimensionless thermal streak spacing (λ^+) has been developed, which is a function of Reynolds (Re) and Prandtl (Pr) number.

The dimensionless thermal streak spacing can be represented as follows.

$$\lambda^+ = \frac{\lambda u^*}{\vartheta} \tag{13}$$

Friction velocity can be represented as follows.

$$u^* = \sqrt{\tau_\omega / \rho} \tag{14}$$

The wall shear stress which is calculated from the pressure drop as follows.

$$\tau_\omega = \frac{\Delta P \times A}{L \times P_s} \tag{15}$$

From the insight of experiments, dimensionless thermal streak spacing is expressed as follows.

$$\lambda^+ = C \times \left(Re^a \times Pr^b \right) \tag{16}$$

The coefficient C, and exponent b are obtained by fitting the test data of present experiments and plotted on dimensionless thermal streak spacing against the Reynolds number and the Prandtl number as shown in Fig. 17.

The obtained equation is given by the relationship

$$\lambda^+ = 2.97 \times \left(Re^{0.45} \times Pr^{0.19} \right) \tag{17}$$

The dimensionless thermal streak spacing predicts the experimental data within ± 15 %.

5 Conclusions

Experiments were performed to study the thermal streak spacing on a heated SS foil cooled by turbulent water flow in a square duct. The measurements were carried out in a range of Reynolds numbers from 5000 to 20000 and Prandtl numbers from 3 to 7. The thermal activity ratio is 0.21 for the entire range of Reynolds and Prandtl numbers. The effects of Reynolds number, Prandtl number and heat flux on the statistics of temperature field, thermal streak spacing and power spectra have been presented and discussed. A new correlation has been proposed to predict thermal streak spacing, which is found to be a function of Reynolds number and Prandtl number. The main conclusions are as follows:

1. Normalized T_{RMS} is found to be increasing with the increase in the Prandtl number. Also, the normalized T_{RMS} increases with the decreasing Reynolds number as temperature amplitude increases with a decrease in Reynolds number.
2. Normalized ΔT_{FW} is found to be slightly increasing with the increase in Prandtl number at fixed Reynolds number. The reason behind that at smaller Prandtl numbers the heat diffuses faster as compared to the velocity (momentum), causing lower ΔT_{FW} for lower Prandtl numbers and vice versa.
3. Also, normalized ΔT_{FW} has been found to be larger at Re of 5000 due to the reduced heat transfer coefficient.
4. The outlet window shows larger ΔT_{FW} and T_{RMS} as compared to the inlet window because the flow is not yet fully thermally developed at the inlet window.
5. The thermal streak spacing and power density decrease with increasing Reynolds number and also decrease with decreasing Prandtl number.
6. A new correlation for the dimensionless thermal streak spacing has been developed that predicts the experimental data with an estimated accuracy of ± 15 %.

Declarations

Conflict of interest On behalf of all authors, the corresponding author states that there is no conflict of interest.

References

1. Roelofs F (2020) Liquid metal thermal hydraulics: State-of-the-art and future perspectives. Nucl Eng Des 362:110590. https://doi.org/10.1016/j.nucengdes.2020.110590

2. Tiselj I, Oder J, Cizelj L (2013) Double-sided cooling of heated slab: Conjugate heat transfer DNS. Int J Heat Mass Transf 66:781–790. https://doi.org/10.1016/j.ijheatmasstransfer.2013.07.076

3. Tiselj I, Cizelj L (2012) DNS of turbulent channel flow with conjugate heat transfer at Prandtl number 0.01. Nucl Eng Des 253:153–160. https://doi.org/10.1016/j.nucengdes.2012.08.008

4. Tiselj I, Horvat A, Mavko B, Pogrebnyak E, Mosyak A, Hetsroni G (2004) Wall properties and heat transfer in near wall turbulent flow. Numer Heat Transf A 46:717–729. https://doi.org/10.1080/104077890504005

5. Kline SJ, Reynolds WC, Schraub FA, Runstandler PW (1967) The structure of turbulent boundary layers. J Fluid Mech 70:741–773. https://doi.org/10.1017/S0022112067001740

6. Boussinesq J (1868) Memoire sur l'influence des frottements dans les mouvements reguliers des fluids. J Math Pures Appl 13(2):377–424

7. Iritani Y, Kasagi N, Hirata M (1985) Heat transfer mechanism and associated turbulent structure in the near-wall region of a turbulent boundary layer. In: 4th Symp on Turbulent Shear Flows, Springer, Berlin, Heidelberg. 223–234 https://doi.org/10.1007/978-3-642-69996-2_18

8. Hetsroni G, Rozenblit R (1994) Heat Transfer to a Liquid-Solid Mixture in a Flume. Int J Multiphase Flow 20:671–689. https://doi.org/10.1016/0301-9322(94)90038-8

9. Hetsroni G, Rozenblit R, Yarin LP (1996) A hot-foil infrared technique for studying the temperature field of a wall. Meas Sci Technol 7:1418–1427. https://doi.org/10.1088/0957-0233/7/10/012

10. Hetsroni G, Zakin JL, Mosyak A (1997) Low-Speed Streaks in Drag-Reduced Turbulent Flow. Phys Fluids 9:2397–2404. https://doi.org/10.1063/1.869469

11. Mosyak A, Pogrebnyak E, Hetsroni G (2001) Effect of constant heat flux boundary condition on wall temperature fluctuations. J Heat Trans ASME 123:213–218 https://doi.org/10.1115/1.1345886

12. Nakamura H, Yamada S (2013) Quantitative evaluation of spatio-temporal heat transfer to a turbulent air flow using a heated thin-foil. Int J Heat Mass Transf 64:892–902. https://doi.org/10.1016/j.ijheatmasstransfer.2013.05.006

13. Shiibara N, Nakamura H, Yamada S (2017) Unsteady characteristics of turbulent heat transfer in a circular pipe upon sudden acceleration and deceleration of flow. Int J Heat Mass Transf 113:490–501. https://doi.org/10.1016/j.ijheatmasstransfer.2017.05.077

14. Nakamura H, Saito R, Yamada S (2020) Delay in response of turbulent heat transfer against acceleration or deceleration of flow in a pipe. Int J Heat Mass Transf 85:108661. https://doi.org/10.1016/j.ijheatfluidflow.2020.108661

15. Tiselj I, Sharma MP, Zajec B, Veljanovski N, Kren J, Cizelj L, Mikuz B (2021) Investigation of turbulent flow in square duct with heated foil thermometry. Int J Heat Mass Transf 175:121381. https://doi.org/10.1016/j.ijheatmasstransfer.2021.121381

16. Düz H (2019) Numerical and experimental study to predict the entrance length in pipe flows. J Appl Fluid Mech 12:155–164. https://doi.org/10.29252/jafm.75.253.29218

17. Bergman TL, Lavine AS, Incropera FP, DeWitt DP (2011) Fundamentals of heat and mass transfer. 7th edition. Wiley

18. Moody LF (1944) Friction factors for pipe flow. Trans. ASME 671-684

19. Incropera FP, DeWitt DP (2001) Fundamentals of Heat and Mass Transfer, 5th edn. John Wiley & Sons, New York

20. Fang X, Xu Y, Zhou Z (2011) New correlations of single-phase friction factor for turbulent pipe flow and evaluation of existing single-phase friction factor correlations. Nucl Eng Des 241(3):897–902. https://doi.org/10.1016/j.nucengdes.2010.12.019

21. Vinuesa R, Schlatter P, Nagib H (2018) Secondary flow in turbulent ducts with increasing aspect ratio. Phys Rev Fluids 3(5):054606. https://doi.org/10.1103/PhysRevFluids.3.054606

22. Uhlmann M, Pinelli A, Kawahara G, Sekimoto A (2007) Marginally turbulent flow in a square duct. J Fluid Mech 588:153–162. https://doi.org/10.1017/S0022112007007604

23. Pirozzoli S, Modesti D, Orlandi P, Grasso F (2018) Turbulence and secondary motions in square duct flow. J Fluid Mech 840:631–655. https://doi.org/10.1017/jfm.2018.66

24. Jones OC (1976) An improvement in the calculation of turbulent friction in rectangular ducts. Trans ASME J Fluids Engg 98:173–181. https://doi.org/10.1115/1.3448250

25. Bergant R, Tiselj I, Hetsroni G (2002) Near-Wall Turbulent Heat Transfer at Prandtl Numbers 1 to 54. Proceedings of the ASME 2002 International Mechanical Engineering Congress and Exposition, New Orleans, Louisiana, USA, November 17–22 36371:57-65. https://doi.org/10.1115/IMECE2002-32006